6 Laser Beam Shaping by Means of Flexible Mirrors

T. Yu. Cherezova, and A. V. Kudryashov

CONTENTS

I. INTRODUCTION

The widespread use of lasers in technological processes highlights the problem of controlling the laser beam parameters. For example, metalcutting processes typically demand the tightest beam focus possible.[1] On the other hand, metalhardening processes require a laser beam with the most uniform transverse irradiance distribution possible.[2] For several laser applications in material processing and manufacturing, nonlinear conversion of a laser beam to a shape with uniform rectangular cross-section is often desirable.[1,2] Examples of such uniform beams include highly multimode laser beams,[3] flattened Gaussian beams,[4,5] and super-Gaussian beams.[6,7]

In general the specified laser irradiance distribution can be formed in different ways — both extracavity[8] and intracavity.[9] The main advantages of intracavity shaping include not only the ability to form the desired irradiance structure, but also the ability to increase the laser output power. One of the most well-known intracavity approaches is to apply graded reflectivity mirrors.[7] However, such mirrors introduce large intrinsic power losses and thus are suitable only in lasers with high-gain active media and generally with unstable resonators. Another intracavity approach is to use graded-phase mirrors.[10,11] However, such mirrors can only serve in the specific applications for which they were designed; every change of laser parameters requires its own unique mirror. A single flexible controlled mirror, on the other hand, can form a number of desired laser outputs. Flexible controlled mirrors can also compensate for various phase distortions caused, for example,

by thermal deformations of resonator mirrors or by aberrations of active media. Uncontrolled phase distortions can destroy the desired laser output distribution. Accurate prediction of phase distortions is not possible because they can depend, for example, on the laser pumping power, the inhomogeneity of the active medium, and so on. For general intracavity beamshaping tasks it is thus easier and more universal to use flexible controlled mirrors.

As the key element of any adaptive optical system, the flexible corrector and its properties determine the performance of the whole system. Demands on the wavefront corrector element include the following:

- A wide range of surface deformation
- A small number of control actuators
- Efficiency of reproducing wavefront aberrations
- Temperature stability of the surface figure
- The ability, if necessary, to conjugate with a wavefront sensor (essential for closed-loop applications)
- Simplicity of fabrication and application
- Low cost

Bimorph mirrors are generally the most suitable correctors to satisfy these demands. It has been shown that semipassive bimorph mirrors with 13 actuators effectively reproduce loworder wavefront aberrations with large amplitudes.[12] For example, bimorph mirrors can theoretically reproduce aberrations with root-mean-square (RMS) amplitudes of the following: defocus: 0.3%, Q1 astigmatism: 0.7%, coma: 5%, and spherical aberration: 6%.

On the other hand, deformable bimorph mirrors are not standard optical elements. They are relatively thin and consist of several different material layers with different properties. As a result, there are no standard optical technologies to produce bimorph mirrors. Special methods of piezoceramic treatment, surface polishing, reflecting coating deposition, and so on, have to be developed to produce highquality bimorph correctors. Some applications of bimorph correctors in lasers and imaging optical systems require an especially wide range of deformation and high stability of the mirror surface. Some of these problems are considered in the next section.

II. DIFFERENT TYPES OF BIMORPH MIRRORS

Pure bimorph mirrors consist of two comparatively thin piezoceramic plates polarized in opposite directions. Manufacturing issues with these pure bimorph flexible mirrors have led to the development of so-called semipassive bimorph correctors.[12,13] A traditional semipassive bimorph mirror consists of two joined plates: a comparatively thick passive glass or metal substrate and a thin active piezoceramic plate (see Figure 6.1). The operational concept for the semipassive bimorph corrector is similar to that for the pure bimorph case, but its sensitivity is lower. Application of an electrical signal to the electrodes of the piezoceramic plate causes tension of the piezodisc due to the inverse piezoelectric effect. The piezodisc thus expands in the radial direction. The bonded substrate prevents free expansion, and this results in bending of the reflective surface. To reproduce different types of aberrations with the help of such a corrector, the outer electrode is divided among several controlling electrodes. The size as well as the number of controlling electrodes depends upon the type of the aberrations to be corrected. Sometimes it is useful to introduce into the mirror design an additional piezodisc with one round electrode for reproducing defocus (Figure 6.1).

Table 6.1 shows the main characteristics for piezoceramic materials that are currently commercially available. Piezoceramic material PKR-7M has the largest value of the piezomodule d_{31}. This material is thus the most sensitive one for the development of bimorph mirrors.

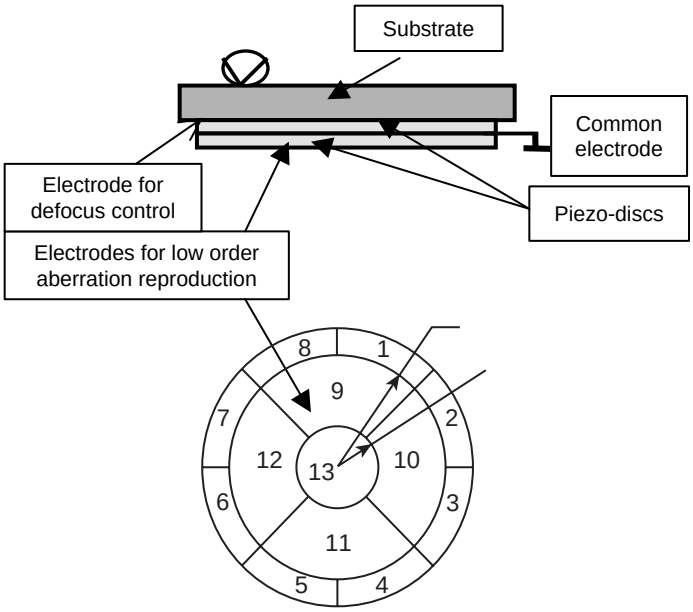

FIGURE 6.1 Design of a semipassive bimorph mirror.

The drawbacks of PKR-7M include a low Curie temperature and the fact that it is a soft segnetomaterial. Since the Curie temperature defines the stability of material properties at high temperatures, a low Curie temperature demands low-temperature technologies for ceramic treatment, bonding of the mirror components, and coating deposition. Q2

Figure 6.2 represents a comparison of the sensitivity of three experimental bimorph mirrors with different types of piezoceramic material. All mirrors include a glass substrate of 2.5 mm thickness and 40 mm aperture and PKR6, PIC151, or PKR-7M ceramic discs of 0.3 mm thickness and 40 mm aperture. The same +100 V potential was applied to the electrodes of the mirrors. Surface deformation dynamics were recorded by a Shack-Hartmann sensor every 50 msec. Sensitivity for the PKR-7M ceramic mirror was 1.4 and 2 times higher than for mirrors with PIC151 and PKR6 ceramics, respectively. For PKR-7M, initial measurements upon application of the control voltage showed 3.2 μm of deformation. This increased to 3.33 μm in 2 sec, then stayed constant for the remainder of the measurement. This indicates that the creep effect for PKP-7M does not exceed 4%.

TABLE 6.1
The Main Characteristics of Piezoceramic Materials

Material	$d_{31} \times 10^{12}$ (C/N)	T_c (°C)	Hardness	α ($\times 10^{-6}$ K^{-1})	Firm Manufacturer
ZTS-19	170	290	hard	~3	ION, Russia
PKR-6	195	300	middle	1–3	Ultrasound Ltd, Russia
PKR-7M	350	175	soft	1–3	Ultrasound Ltd, Russia
PZT-5H	275	193	soft	1.5	Morgan Matroc, UK
PZT-5A	171	365	middle	1.5–2	Morgan Matroc, UK
PIC-151	210	250	middle	—	Physik Instrumente, Germany
P1 94	305	185	soft	—	Quartz & Silica, France
PCM-33A	262	—	soft	—	Matsushita Electric, Japan

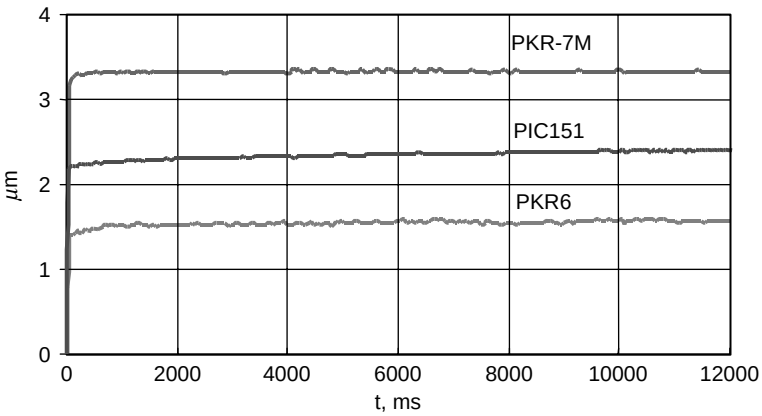

FIGURE 6.2 Deformation of bimorph mirrors made from different piezoceramic materials vs. time.

Typical ceramic hysteresis curves exhibit a "butterfly" pattern (Figure 6.3). Depolarization or even reverse polarization phenomena occur at potentials opposite to the polarization direction voltage. We measured the threshold negative voltage at which depolarization begins for PKR-7M, which equals -500 V per mm of ceramic. To avoid unpredictable behavior of the mirror deformation, the range of negative control voltage should be restricted. For example, the range of control voltage for a 0.4 mm thickness ceramic could be varied from -200 to $+300$ V. The response of the bimorph actuator remains linear within this range (Figure 6.4).

One of the important characteristics of correctors is the temperature stability of the mirror reflecting surface. Surface instability is basically caused by the difference between the thermal expansion coefficients for substrate material α_1 and piezoceramic material α_2. In the simplest cases, the instability behavior manifests itself in additional defocus deformation of the mirror surface due to changes in ambient temperature.

Application of an additional voltage to the electrodes of the piezodisc $V_{\Delta T} = (t/d_{31}) \times (\alpha_1 - \alpha_2)\Delta T$ can compensate for thermal deformation. This limits the dynamic range of the control voltage. For example, for a copper substrate ($\alpha_1 = 15.9 \times 10^{-6}\ \mathrm{K}^{-1}$), almost 20% of the maximal

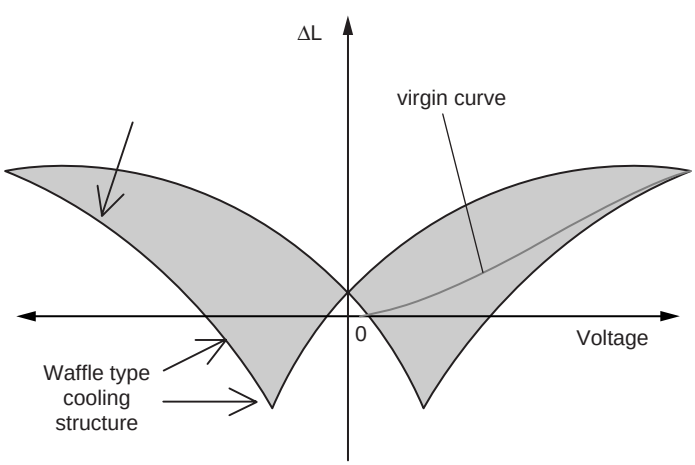

FIGURE 6.3 Response of a PZT actuator to a bipolar drive voltage.

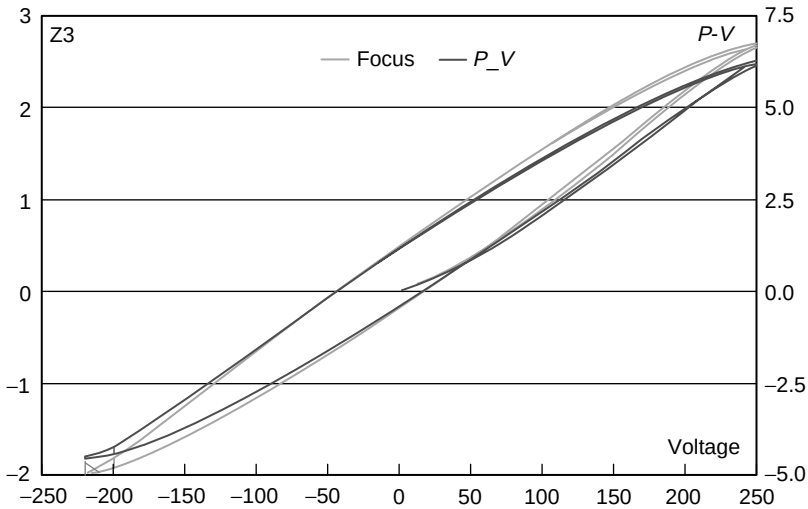

FIGURE 6.4 Hysteresis curve for a 40 mm bimorph mirror. The *y*-axis represents the value of mirror deformation $P-V$ (peak-to-valley) measured in μm; the *x*-axis represents the voltage given in volts.

range of the control voltage would be used to compensate for thermal deformation caused by a 5 °C change in temperature.

The main criterion for the choice of a substrate material is the thermal expansion value α_1, which should be close to α_2 for the chosen piezoceramic material ($\sim 3 \times 10^{-6}\ \mathrm{K}^{-1}$). Table 6.2 shows the parameters of optical materials, which are used in the manufacturing of experimental samples of bimorph mirrors. Piezoceramic lead–zinconate–titanate (PZT) is the most suitable material for a mirror substrate. In this case, we can ensure equality of thermal expansion coefficients, leading to an ideal mirror for thermal stability. However, there can also be problems with polishing ceramic materials that have a tendency to crumble. Ceramic material PKR-7M, which is produced under special heat baking technology, allows polishing of the surface to optical quality.

Another method for thermally stabilizing the mirror shape is water-cooling. Water-cooling is very important in high power laser applications, where the mirror is heated by the laser beam. In this case, channels for cooling water circulation have to be formed inside the thin substrate

TABLE 6.2
Parameters of Materials for Mirror Substrates

	Parameters					
Material	**Density, g (kg/m^3)**	**Index of refraction**	**Index of a thermal expansion, α ($\times 10^{-6}$ K^{-1})**	**The module of the Young, E (Pa $\times 10^{-9}$)**	**Thermal conductivity, β (W/(m K))**	**Specific thermal capacity (J/(kg K))**
Quartz glasses KU1, KU2, KU	2.2	1.46	0.55	98	1.36	733
Optical glass LK-5	2.27	1.4846	3.5	69	1.2	—
Piezoceramics PZT	7.4–7.7	—	1–3	46–90	1.4	400
Monocristalline Si	2.33	3.3	2.54	126–131	150	700
Copper Cu	8.96	—	15.9	129.5	401	385

of the mirror (see Figure 6.5). We are producing such cooled mirrors from copper, because copper is a good material for machining, diffusion welding, and optical polishing. Such cooled mirrors are used for formation and correction of continuous wave (CW) CO_2 laser beams with powers up to 5 kW.[13]

Figure 6.6 shows experimental samples of bimorph mirrors that we have developed for different applications. Mirror apertures varies from 30 to 100 mm. The number of control electrodes on the mirrors varies from 17 to 33. The mirror surfaces were deposited with multilayer dielectric and protected silver coatings. These coated mirrors were subjected to beam irradiances up to $\sim 10^{12}$ W/cm^2 without observable damage.

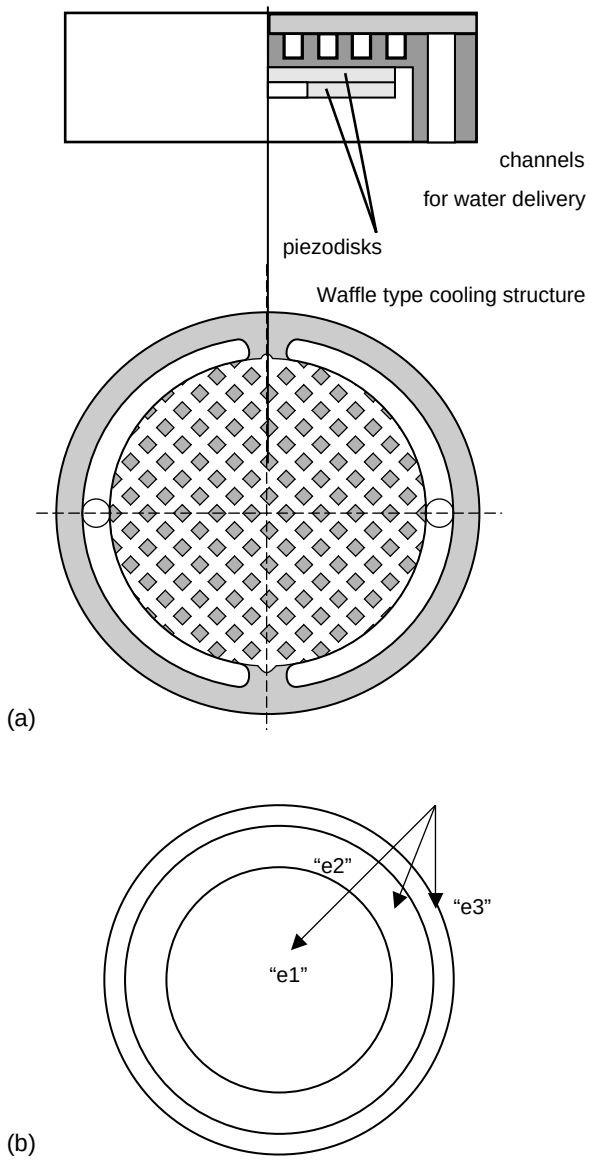

FIGURE 6.5 Sample of cooling structure for a water-cooled bimorph mirror; (b) layout of mirror electrodes (e1 is underneath e2 and e3).

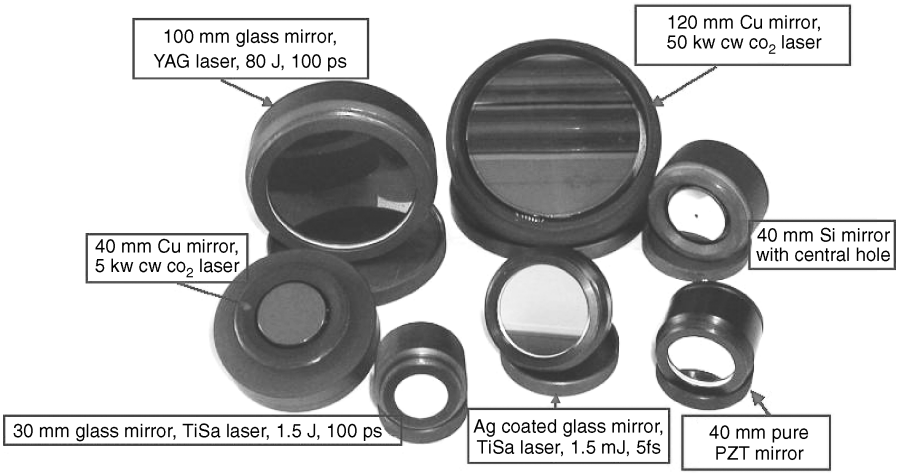

FIGURE 6.6 Photograph of experimental bimorph mirrors.

The 30 mm aperture bimorph mirror shown in Figure 6.6 is used for the formation of the near-field laser beam distribution for the last amplifier of the ATLAS Ti:Sa laser at MPQ, Garching, Germany.[14] The homogenizing of the irradiance distribution produced by this flexible mirror allowed pulse energy to increase from 0.5 to 1.5 J. The next mirror, shown in Figure 6.6, having an 80 mm aperture and 33 control actuators, is used in the same laser for far-field wavefront correction. Closed-loop control of the mirror produced an almost diffraction-limited spot at the focal plane of the nonaxial parabolic mirror.

In addition to their utility for extracavity beam correction and formation, bimorph mirrors are very useful in intracavity applications. The following sections detail an investigation of bimorph correctors for intracavity laser beam formation. For intracavity applications, we suggest the use of the well-developed water-cooled flexible mirror designs (Figure 6.5) to avoid any undesirable surface thermal deformations. As Figure 6.5 illustrates, such mirror designs contain two piezodiscs, where the interface between the piezoceramic discs contains a continuous conducting 'ground' electrode. Another continuous conducting electrode between the piezodisc and the copper plate e1is used to control the overall curvature of the entire mirror. Two controlling electrodes, e2 and e3, having the form of concentric rings, were attached to the outer surface of the piezodisc. The response function for each mirror electrode (the deformation of the mirror surface while applying voltage to each mirror electrode) is shown in Figure 6.7 and was measured using a modified Fizeau interferometer.[15] Three-dimensional profiles of the response functions are shown in Figure 6.8. These response functions will be used in the intracavity procedures described in this chapter.

Q4

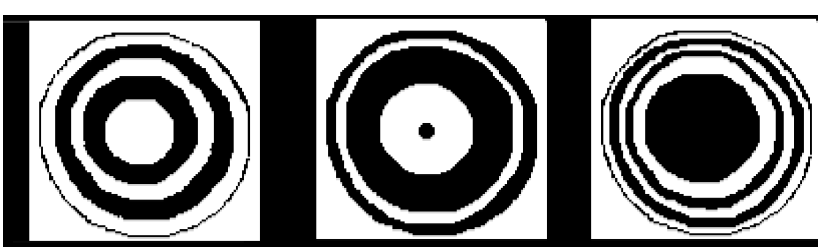

FIGURE 6.7 Level map of response functions of three electrodes: (a) common focus–defocus electrode e1 ($P - V = 0.81\ \mu$ for applied voltage 20 V); (b) second ring electrode e3 ($P - V = 0.35\ \mu$ for applied voltage 40 V); (c) first ring electrode e2 ($P - V = 0.79\ \mu$ for applied voltage 40 V).

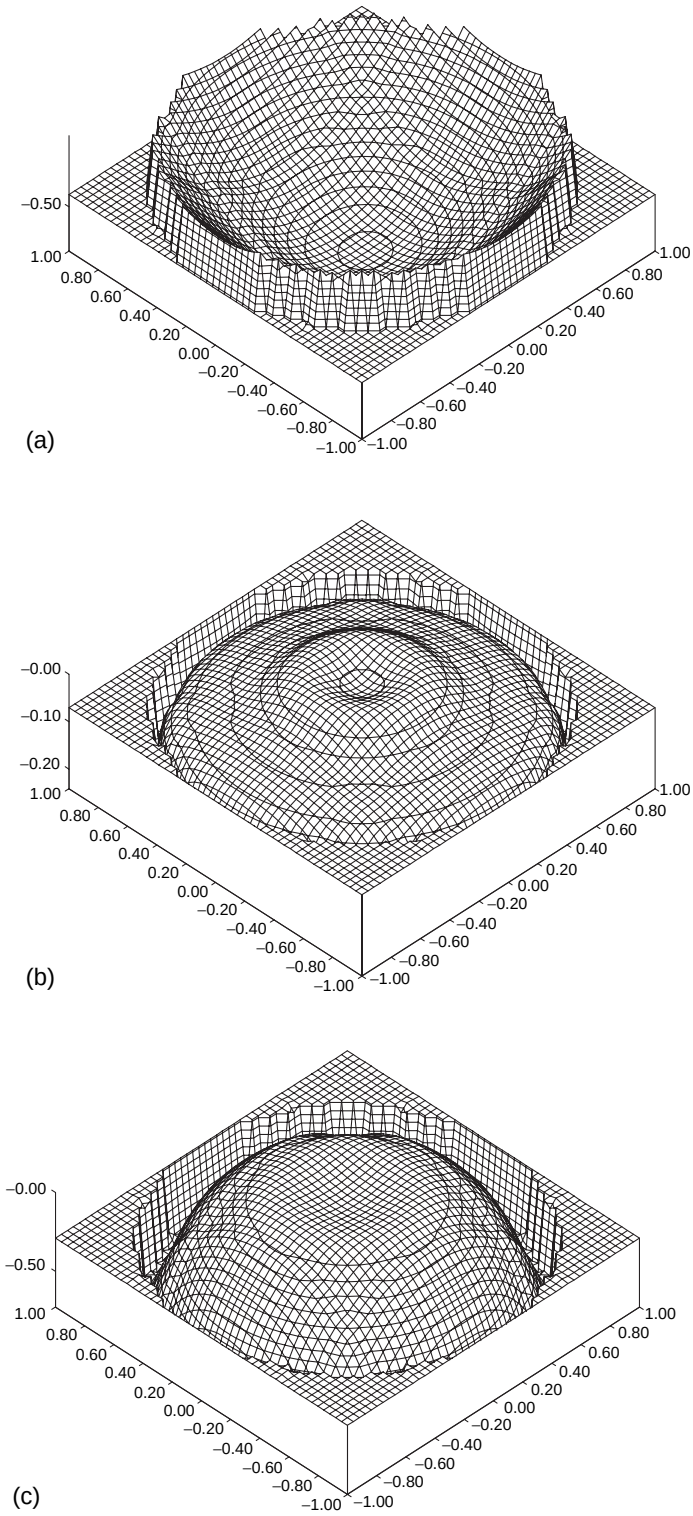

FIGURE 6.8 Surface profiles of an adaptive mirror: (a) for common focus–defocus electrode e1 — applied voltage is 20 V, (b) for second ring e3 — applied voltage is 40 V, (c) for first ring of electrodes e2 — applied voltage is 40 V.

III. FORMATION OF A DESIRED LASER BEAM AT THE LASER RESONATOR OUTPUT BY MEANS OF AN INTRACAVITY FLEXIBLE CORRECTOR

For many industrial applications it is desirable to have the laser generating a single, mostly fundamental mode and to have good power extraction at the same time. Gaussian beams are relatively narrow and therefore result in poor energy extraction. We would thus expect that the formation of a wider super-Gaussian irradiance distribution inside the laser cavity would lead to an increase in the active medium gain extraction.

The algorithm for the desired irradiance formation as well as the numerical results will be discussed using a stable laser cavity (Figure 6.9). Such a cavity corresponds to the industrial continuous discharge CO_2 laser ILGN-704 produced by Istok (Fryazino, Russia). The geometry of the resonator consists of a plane output coupler and an active mirror separated from the coupler by the distance $L = 2$ m.

Azimutal symmetry can be assumed, which allows us to use the one-dimensional Huygens–Fresnel integral equations[16,17] to calculate the amplitude of a mode in the empty laser resonator;

$$\gamma_2 \Psi_2(r_2) = \int_0^b K_1(r_1, r_2)\Psi_1(r_1) r_1 \mathrm{d}r_1 \tag{6.1}$$

$$\gamma_1 \Psi_1(r_1) = \int_0^a K_2(r_2, r_1)\Psi_2(r_2) r_2 \mathrm{d}r_2 \tag{6.2}$$

where γ_i is the eigenvalue and $\Psi_i(r_i)$ is the eigenmode of the resonator, r_i is a radial co-ordinate, $i = 1$ indicates a plane output mirror of diameter $2b$, and $i = 2$ indicates an active mirror of diameter $2a$. These lead to:

$$K_1(r_1, r_2) = \frac{j}{B} J_l\left(k\frac{r_1 r_2}{B}\right) \exp\left(-\frac{jk}{2B}\left(Ar_1^2 + Dr_2^2\right)\right) \tag{6.3}$$

$$K_2(r_2, r_1) = \frac{j}{B} J_l\left(k\frac{r_1 r_2}{B}\right) \exp\left(-\frac{jk}{2B}\left(Ar_1^2 + Dr_2^2\right)\right) \exp\left(jk\varphi_{\mathrm{mirror}}(r_2)\right) \tag{6.4}$$

Here, J_l is the Bessel function of order l (we take into account only the lowest transverse mode with $l = 0$), and A, B, C, and D are the constants determined by the $ABCD$ ray matrix of the laser resonator. We consider an empty resonator, so that $A = 1$, $B = L$, $C = 0$, and $D = 1$.

The algorithm to form the desired irradiance distribution is the so-called "inverse propagation method" described in several references.[11,18–21] The desired output field distribution $\Psi_1(r, \varphi)$ is specified on the output mirror. The back-propagation of the laser beam through all the resonator's

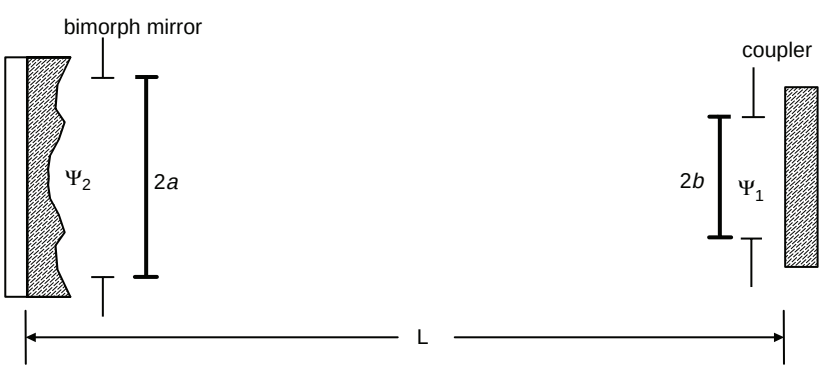

FIGURE 6.9 Schematic setup of the CW CO_2 laser with adaptive mirror.

elements to the active corrector is calculated using the Huygens-Fresnel integral equations (Equation 6.1 and Equation 6.2). In the plane of the active corrector, the wavefront is calculated to determine the appropriate mirror phase profile $\varphi_{\text{mirror}}(r)$:

$$\varphi_{\text{mirror}}(r) = -\varphi_{\text{beam}}(r) \tag{6.5}$$

An ideal corrector (graded-phase mirror) could completely reconstruct such a phase profile.[11,18–21] In our case, bimorph mirrors can approximate the necessary phase profile with some small degree of error. This RMS error can be calculated using the experimentally measured response functions of the mirror. In other words:

$$\left(Z(r) - \sum_{i=1}^{i=3} U_i F_i(r)\right)^2 \longrightarrow \min \tag{6.6}$$

where $Z(r)$ is the profile to be reconstructed, $F_i(r)$ are response functions of the flexible mirror electrodes given in Figures 6.7 and 6.8, and U_i are weight coefficients corresponding to the voltages applied to each electrode.

The left side of Equation 6.6 has a minimum when its first derivative equals zero:

$$\frac{\partial}{\partial K_i}\left(Z(r) - \sum_{i=1}^{i=3} U_i F_i(r)\right)^2 = 0 \tag{6.7}$$

Equation 6.7 then determines the applied voltages to approximate the necessary shape of the laser beam.

The procedure described above gives us the reconstructed mirror surface $\varphi_{\text{mirror}}(r)$ which is substituted into Equation 6.4. To solve the integral equations (Equation 6.1 and Equation 6.2) we used the Fox and Li iterative method of successive approximations[16,17] to take into account edge diffraction as well as nonideal reproduction of the necessary phase profile by the bimorph flexible mirror.

IV. MAIN RESULTS

The main parameters of the laser resonator (Figure 6.9) are the Fresnel numbers $N_1 = b^2/(B\lambda)$ and $N_2 = a^2/(B\lambda)$, and the geometrical factor $G = (1 - L/R_2)$; where $\lambda = 10.6\ \mu$m is wavelength, $R_2 = 4$ m is the radius of curvature of the active mirror, and $L = 2$ m is the length of the resonator cavity. The initial field distribution on the planar output coupler is chosen as $\Psi(r) = \exp(-(r/W)^n)$, where n determines the order of the super-Gaussian function and W is the beam waist. The particular beam waist is chosen according to the methods of moments for laser beams[21]:

$$w^2 = \left(M^2 \frac{\lambda L}{2\pi}\right)\left(\frac{1+G}{1-G}\right)^{1/2} \tag{6.8}$$

where M^2 is the beam quality factor:

$$M^2 = \frac{(w\theta)_{\text{mode}}}{(w\theta)_{\text{TEM}_{00}}} \tag{6.9}$$

A. Formation of a super-Gaussian Beam of the Fourth Order ($n = 4$)

From Equation 6.8 and Equation 6.9, the super-Gaussian beam waist is calculated: $W = 3.1$ mm. Figure 6.10(a) represents the phase distribution of a super-Gaussian beam (curve 1)

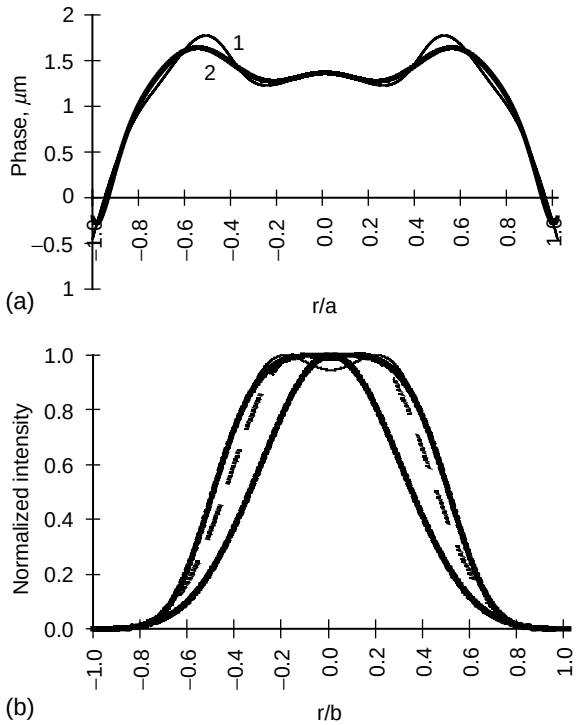

FIGURE 6.10 Formation of a super-Gaussian beam of the fourth order, $N_1 = 1$, $N_2 = 4.7$, $G = 0.5$: (a) 1 (solid curve) — the phase profile of the laser beam to be reconstructed and 2 (dashed) — the phase profile of the flexible mirror; (b) normalized irradiance distributions on plane coupler: 1 — Gaussian irradiance distribution, corresponding to the same geometry of resonator but with a spherical mirror, 2 — the desired super-Gaussian irradiance profile, 3 — irradiance formed by graded-phase mirror, 4 (dashed) — by bimorph flexible one.

back-propagated through the resonator starting at the output coupler and going a distance of $L = 2$ m to the adaptive mirror. Curve 2 (Figure 6.10(a)) illustrates the phase profile of the active mirror reproducing the phase shape of laser beam with an RMS error of 0.3%. Figure 6.10(b) shows the beam irradiance distribution at the output coupler for various resonator conditions. Curve 1 corresponds to the fundamental Gaussian mode of the same resonator, but with a pure spherical mirror. Curve 2 (solid) shows the desired super-Gaussian relative irradiance profile, while curve 3 shows the profile produced with an ideal corrector (graded-phase mirror with no deviation from the necessary phase profile). Finally, curve 4 corresponds to the irradiance distribution in the resonator with an adaptive mirror.

One may see from Figure 6.10(b) that applying the active corrector (curve 4) increases the output mode volume by 1.5 times in comparison with a pure Gaussian beam (curve 1). At the same time, diffraction losses per transit decrease by 1.7 times. The voltages applied to each electrode were calculated from Equation 6.7 and are given in Table 6.3.

Users of lasers often dislike super-Gaussian irradiance distributions for their side lobes in far-field patterns. However, the shaped super-Gaussian distribution is not exactly the super-Gaussian function: its form has been changed by edge diffraction and by the nonideal behavior of the active mirror in forming the necessary phase profile. That is why the side lobes of the beam formed by an active mirror contain only 2% of the total energy (dashed curve 3 in Figure 6.11). This irradiance profile is thus very attractive for industrial applications. For comparison, curve 2 in Figure 6.11(a) and (b) represents the far-field pattern for a super-Gaussian beam formed by an ideal (graded-phase) corrector.

TABLE 6.3
Voltages (V) Applied to the Electrodes of a Bimorph Flexible Mirror

n, order of the given super-Gaussian beam formation	e1	e2	e3
4	−64	−116	71
6	−107	−300	−240
8	−43	−214	−171

B. Formation of a super-Gaussian Beam of the Sixth Order ($n = 6$)

In this case, the beam waist of the desired super-Gaussian distribution is chosen as 3.3 mm. Figure 6.12(a) represents the exact phase distribution of the desired super-Gaussian beam and the phase profile of a flexible mirror (RMS error of the approximation is about 0.1%). Figure 6.12(b) shows irradiance distributions formed by the flexible mirror at the output coupler. The far-field results are very close to those for the fourth-order super-Gaussian beam represented in Figure 6.11(a) and (b). Mirror electrode voltages calculated from Equation 6.7 are presented in Table 6.2.

For this case, the output mode volume increases by a factor of 1.3 in comparison with a pure Gaussian beam while diffraction losses per transit decrease by 1.5 times.

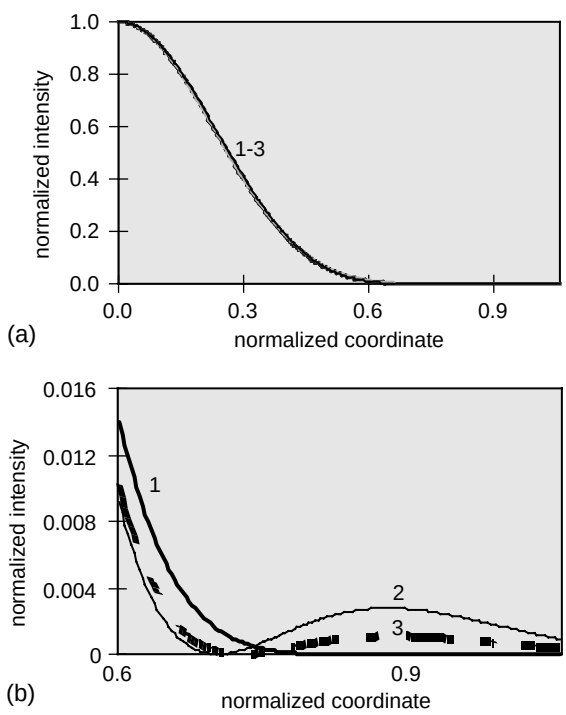

FIGURE 6.11 Formation of a super-Gaussian beam profile of the fourth order. (a) Normalized irradiance distributions in the far-field zone: 1 — Gaussian beam, 2 — beam formed by ideal corrector (graded-phase mirror), 3 (dashed curve) — beam formed by active mirror; (b) fragment near the edge of the same irradiance distributions.

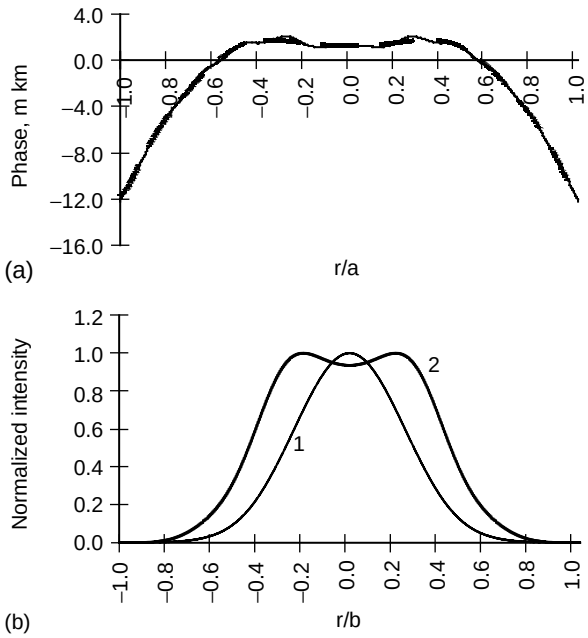

FIGURE 6.12 Formation of a super-Gaussian beam profile of the sixth order, $N_1 = 1, N_2 = 14.1, G = 0.5$. (a) (solid) — phase profile of laser beam to be reconstructed and (dashed) — phase profile of bimorph mirror; (b) normalized irradiance distributions: 1 — Gaussian TEM_{00} mode for the same resonator but with a pure spherical bimorph mirror, 2 — sixth order super-Gaussian beam formed by the bimorph flexible mirror.

C. Formation of a super-Gaussian Beam of the Eighth Order ($n = 8$)

For this case, the beam waist of the desired eighth-order super-Gaussian fundamental mode is equal to 3.5 mm. The main results are given in Figure 6.13(a) and (b). The output mode volume increased 1.6 times in comparison with a pure Gaussian beam, while diffraction losses per transit decrease by a factor of 1.7. Although the flexible mirror error in producing the desired phase shape is relatively low (RMS error $< 0.1\%$), it could not exactly reproduce the two main humps (Figure 6.13(a)). However, if the controlling electrode's position could be matched to the co-ordinates of the two local maxima (Figure 6.13(a), solid curve), such an active corrector would be able to reproduce the shape more accurately. Applied mirror electrode voltages are again given in Table 6.2.

It should be mentioned that active mirrors sometimes produce a smoother phase profile than is desirable for higher-order modes. This situation can lead to higher diffraction losses for the TEM_{00} mode than for the TEM_{01} mode, which causes the laser to resonate in the TEM_{01} or some combination of higher-order modes. In contrast, an ideal corrector, such as a graded-phase mirror, tends to disturb the higher-order modes to a greater extent, which causes higher diffraction losses and thus suppresses their amplitude in the cavity.[18] This is confirmed by Figure 6.14, which shows the irradiance distribution of a TEM_{01} mode on the output coupler where an eighth-order super-Gaussian beam is desired. The TEM_{01} mode, shaped by an ideal corrector (curve 1 in Figure 6.14) and by an active corrector (curve 2), is shown. One may see the irradiance of the TEM_{01} mode in the first case is more distorted; hence, its diffraction losses are higher. As an example, for the previously given resonator parameters and a bimorph active corrector, diffraction losses per transit of the super-Gaussian mode formed by a bimorph mirror are $(1 - |\gamma_1\gamma_2|) = 4.4 \times 10^{-5}\%$, while for the TEM_{01} the losses are $(1 - |\gamma_1\gamma_2|) = 2 \times 10^{-5}\%$. To increase the discrimination between transverse modes one needs to perform an optimization procedure.

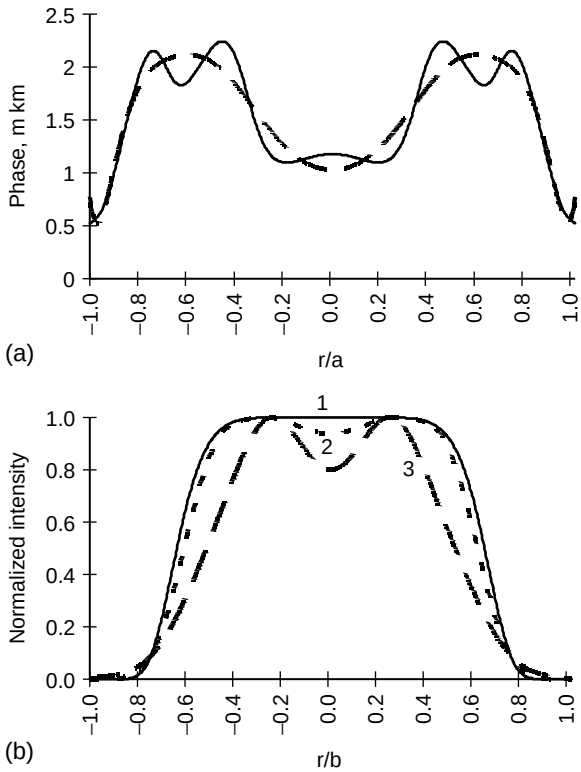

FIGURE 6.13 Formation of a super-Gaussian beam profile of order eight, $N_1 = 1$, $N_2 = 4.7$, $G = 0.5$. (a) (solid) — the phase profile of the given laser beam at the position of bimorph mirror and (dashed) — phase profile of the mirror; (b) normalized irradiance distributions: 1 (solid) — the desired super-Gaussian beam, 2 (dotted) — irradiance produced with a graded-phase mirror, 3 (dashed) — irradiance produced with bimorph flexible mirror.

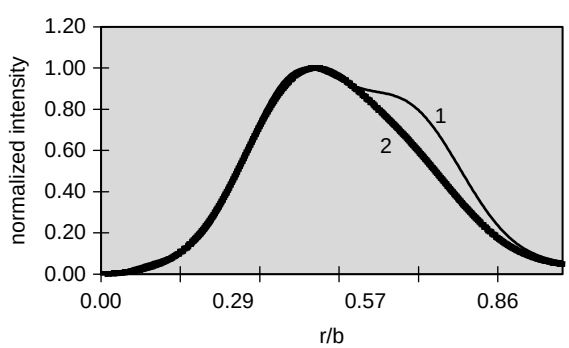

FIGURE 6.14 Normalized irradiance distribution of TEM_{01} mode while forming an eighth-order super-Gaussian fundamental mode: 1 — ideal corrector (such as a graded-phase mirror), 2 — bimorph flexible mirror.

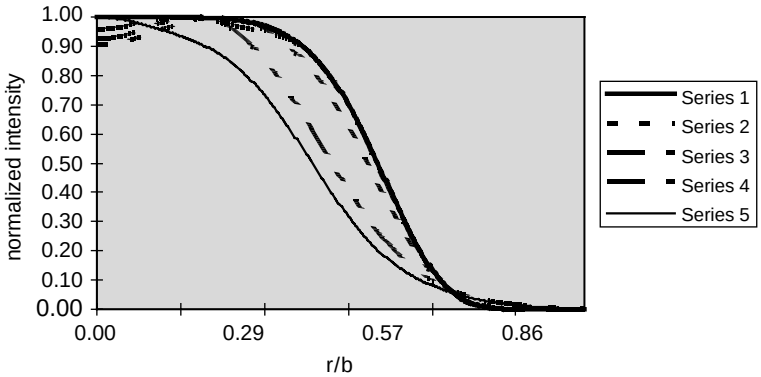

FIGURE 6.15 Normalized irradiance profiles on the plane output coupler for the sixth-order super-Gaussian fundamental mode. Series 1: the desired beam; Series 2: $N_2 = 4.7$; Series 3: $N_2 = 6.8$; Series 4: $N_2 = 10$ (very close to the desired beam except at the center); Series 5: $N_2 = 14.1$, $N_1 = 1$, $G = 0.5$.

D. Optimization of Laser Parameters

The optimization of the laser resonator parameters N_2 (Fresnel number) and G (geometric factor) was carried out in order to produce the closest match to the desired irradiance distribution. Figure 6.15 shows the normalized output irradiance profiles produced by varying N_2 from 4.7 to 14.1 ($N_1 = 1, G = 0.5$). Note that for the graded-phase mirror, the best result is reached when the Fresnel number N_2 is a maximum. This is understandable: increasing N_2 corresponds to enlarging the size of an aperture in front of the graded-phase mirror (see Figure 6.9), which causes a more complete approximation of the incident resonator mode shape by this mirror. As a result, the output profile is closer to what is desired. In contrast, for an active corrector with given electrode axial positions, an increase in N_2 does not necessarily lead to better performance. For example, one may see from Figure 6.15 that for $N_2 = 10$ (series 4) the obtained irradiance distribution is very close to the desired one. Also, a rather good approximation to the desired super-Gaussian curve was obtained for $N_2 = 4.7$ (series 2, Figure 6.15). However, for the highest Fresnel number $N_2 = 14.1$ (series 5, Figure 6.15) the shape of the obtained output profile is not as good as for lower Fresnel numbers. This is because the fixed electrodes may have difficulty replicating a larger incident mode profile, and in fact may have to make compromises in the center of the mirror where the majority of the incident mode amplitude is concentrated.

Another parameter that must be taken into consideration is diffraction losses per transit. We calculated such losses for the eighth-order super-Gaussian fundamental mode and the results are presented in Figure 6.16. The curve has a minimum for $N_2 = 6.8$. In that case, the bimorph flexible mirror does the best job of reproducing the resonator mode shape. At this minimum point, the diffraction losses of TEM_{01} mode are approximately ten times higher than the TEM_{00} mode. The obtained irradiance curves do not depend upon the variation of G, because the active mirror can reproduce focus (or defocus) very well (mainly by applying a voltage to the common focus–defocus electrode; Figures 6.7 and 6.8).

V. FORMATION OF AN ANNULAR BEAM

To solve various tasks in modern laser physics and nonlinear optics, it is sometimes necessary to have beam profiles that differ from a uniform profile. For example, to deliver high-power laser radiation through the atmosphere, it is desirable to form an annular laser beam with a planar phase distribution because it has less nonlinear distortion in nonlinear and turbulent media than other

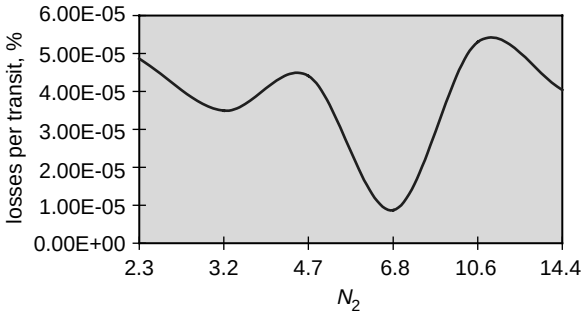

FIGURE 6.16 Diffraction losses per transit for an eighth-order super-Gaussian fundamental mode in a resonator with an active corrector. $N_1 = 1$, $G = 0.5$.

forms of laser beams.[22,23] The traditional way to form such a beam is to obscure the central part of a Gaussian fundamental mode. However, in this case we have additional power losses. As is shown below, an intracavity active mirror allows us to form an annular beam without any additional power losses and with less diffraction losses than for a traditional Gaussian fundamental mode.

The desired initial field distribution for the annular beam at the plane output coupler of a laser resonator (Figure 6.9) is chosen as $\Psi_1(r_1) = \{(r + 0.1)/3.1\}2\exp(-((r + 0.1)/3.1)^4)$. A small decentration value, in this case 0.1 mm, had to be added so that diffraction did not drastically change the desired annular irradiance shape of the fundamental mode during Fox–Li numerical calculations.[16,17] The main parameters of the laser resonator were Fresnel numbers $N_1 = b^2/(B\lambda) = 1$, $N_2 = a^2/(B\lambda) = 4.7$, and geometrical factor $G = (1 - L/R_2) = 0.5$, where $R_2 = 4$ m is the radius of curvature of the flexible mirror and $L = 2$ m is the length of the resonator cavity.

Figure 6.17(a) represents the phase distribution of the annular beam propagated back to the flexible mirror at the distance $L = 2$ m from the output plane mirror (gray curve). The smoother,

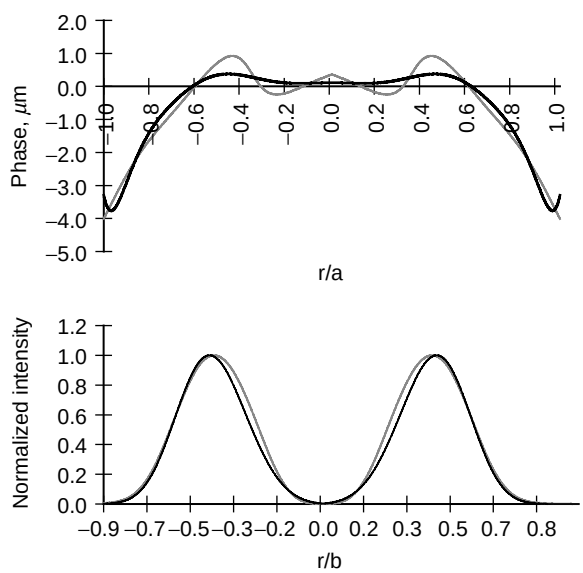

FIGURE 6.17 Formation of a doughnut-like beam: $N_1 = 1$, $N_2 = 4.7$, $G = 0.5$: (a) (gray curve) the phase profile of the laser mode to be reconstructed and (black) the phase profile of the bimorph flexible mirror; (b) normalized irradiance distributions on the plane output coupler: (black) the desired irradiance profile and (gray) irradiance profile formed by the flexible mirror.

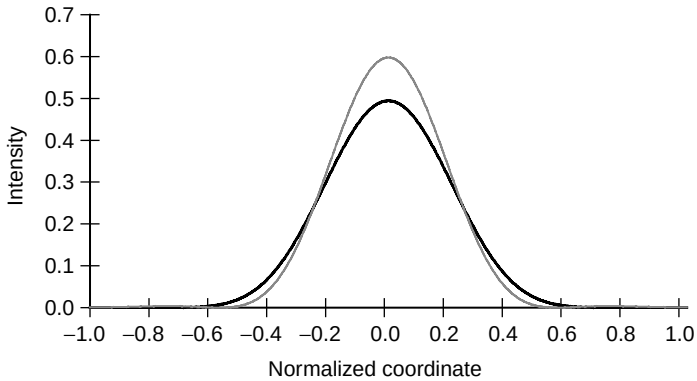

FIGURE 6.18 Irradiance distributions in the far-field: (black) far-field pattern of a Gaussian fundamental mode, (gray) far-field pattern of the doughnut-like beam.

black curve of Figure 6.17(a) illustrates the phase profile of the bimorph flexible mirror reproducing the phase shape of the laser beam with RMS error 0.7%. Figure 6.17(b) shows irradiance distributions on the plane output coupler. The black curve corresponds to the desired irradiance profile and the gray curve to the profile formed by the intracavity flexible mirror. The diffraction losses of the annular beam were estimated as $\delta = |1 - \gamma_1\gamma_2|$, where γ_1, γ_2 are the eigenvalues defined from Equation 6.1 and Equation 6.2. Such losses decreased by a factor of 1.4 in comparison with a Gaussian TEM_{00} mode.

The far-field pattern of this annular beam contains about 96% of its total energy in the main lobe (as shown by the gray curve in Figure 6.18). With a beam quality factor $M^2 = 1.2$, this irradiance profile is very attractive for industrial applications. For comparison we plotted the far-field pattern for a Gaussian fundamental mode from the same resonator. The edges of the far-field intensities are shown in Figure 6.19 in expanded scale, showing a small amount of energy in the second diffraction ring for the annular beam. The voltages applied to each electrode to form the annular fundamental mode are given in Table 6.4.

VI. EXPERIMENTAL FORMATION OF A SUPER-GAUSSIAN BEAM BY MEANS OF BIMORPH FLEXIBLE MIRROR

The experimental formation of a specified beam, namely a super-Gaussian of fourth and sixth orders, was performed using an industrial fast axial flow continuous-discharge CO_2 laser with

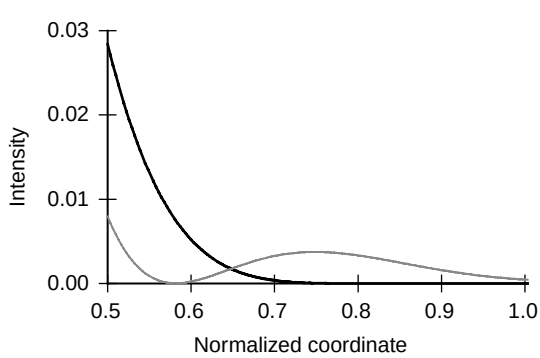

FIGURE 6.19 The fragment near the beam edge for the irradiance distributions shown in Figure 6.18.

TABLE 6.4
Voltages (V) Applied to the Electrodes of a Flexible Mirror to Form an Annular Beam

e1	e2	e3	e4
−47.5	−254	0	0.7

a stable resonator, produced by IPLIT, Russian Academy of Sciences, model TLA-600.[24] The laser resonator (Figure 6.20) consists of a plane output coupler (7), a CO_2 gain tube (6), convex (5) and concave (4) mirrors, and the bimorph flexible mirror (2).

First of all, in order to model the behavior of the cavity with our flexible mirror and to determine the mirror electrode voltages to form super-Gaussian beams of fourth and sixth orders, we perform all of the numerical calculations described in Equation 6.1 to Equation 6.7. However, in the case of a real laser having an active medium (not just an empty resonator as it was before), we must take into account active medium saturation caused by the intense beam. That is why the kernels of integral Equation 6.1 and Equation 6.2, given by Equation 6.3 and Equation 6.4, have the additional multiplier $H(I)$ taking into account this effect:

$$K_1(r_1, r_2) = 2\pi \frac{j}{\lambda B} J_0\left(k\frac{r_1 r_2}{B}\right) \exp\left(-\frac{jk}{2B}(Ar_1^2 + Dr_2^2)\right) H(I) \tag{6.10}$$

and

$$K_2(r_2, r_1) = 2\pi \frac{j}{\lambda B} J_0\left(k\frac{r_1 r_2}{B}\right) \exp\left(-\frac{jk}{2B}(Ar_1^2 + Dr_2^2)\right) \exp\left(jk\varphi_{\text{mirror}}(r_2)\right) H(I) \tag{6.11}$$

where

$$H(I) = \left(1 + \frac{g_0 L_{\text{am}}}{2\left(1 + \frac{I(r)}{I_s}\right)}\right) \tag{6.12}$$

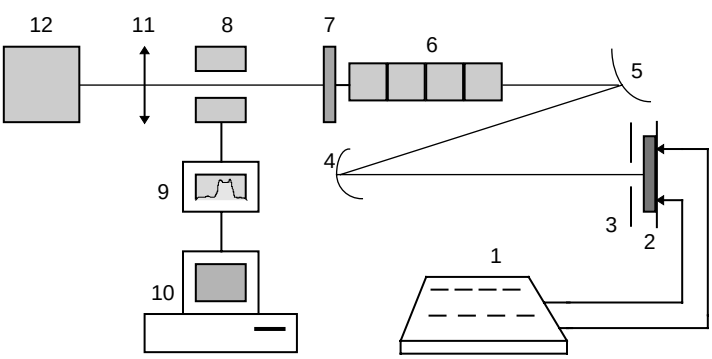

FIGURE 6.20 Schematic of the experimental setup to form a super-Gaussian TEM_{00} mode: 1 — variable-voltage power supply for controlling mirror electrodes, 2 — semipassive bimorph mirror, 3 — diaphragm, 4 — concave mirror $R = 2200$ mm, 5 — convex mirror $R = -800$ mm, 6 — active CO_2 gain medium, 7 — ZnSe output mirror with coefficient of reflectivity 69%, 8 — LBA-2A (laser beam analyzer), 9 — oscilloscope, 10 — computer, 11 — lens $f = 275$ mm, 12 — MAC-2 (mode analyze computer).

Here g_0 is the small-signal gain coefficient; $g_0 = 110\ \text{cm}^{-1}$ for this particular type of laser.[24] L_{am} is the length of the active medium ($L_{am} = 80$ cm), $I(r)$ is the transverse irradiance distribution of the laser beam, and I_s is the saturation irradiance ($I_s = 110\ \text{W/mm}^2$). If the irradiance of the laser beam $I(r)$ becomes comparable with I_s (saturation irradiance of the active medium), then the overall irradiance of the laser beam becomes lower.

The main resonator parameters for the CO_2 laser shown in Figure 6.20 are Fresnel numbers $N_1 = b^2/\lambda B = 0.66$ and $N_2 = a^2/\lambda B = 6.47$, and stability factor $G = 0.51$ (here $b = 8$ mm, the radius of the plane output mirror; $a = 25$ mm, the radius of bimorph mirror; $\lambda = 10.6\ \mu$m, the wavelength; and $B = 9104$ mm, the effective length of the resonator). Parameters of the super-Gaussian function $\Psi(r) = \exp(-(r/W)^n)$ are chosen as $W = 4.8$ mm and $W = 5.1$ mm for $n = 4$ and $n = 6$, respectively. The particular beam waists were chosen according to the theory of moments and are well described in Bélanger and Paré.[21] For this laser, we can assume $H(I)$ =constant, since the irradiance of the beam is much smaller than the saturation irradiance I_s of the active medium. The voltages at the flexible mirror electrodes needed to form the super-Gaussian beams were calculated according to the algorithm described earlier in Chapter 3.

Figure 6.21 shows the evolution of the fourth-order super-Gaussian beam at the surface of output mirror as a function of the round trip number, based on numerical calculations. Curve number 1 represents the original beam, while the other curves show beam profiles after a corresponding number of round trip passes calculated from Equation 6.2 to Equation 6.5. Given the resonator parameters mentioned previously in this section, we need to make about 130 iterations to reach a convergence point where successive calculations differ by less than 10^{-7}.

Figure 6.22(a) and (b) show the main results of the calculations: the Gaussian (curve 1) and super-Gaussian of the fourth- and sixth-order fundamental mode irradiance distributions (curve 2) on the plane output mirror. The far-field pattern for the calculated fourth-order super-Gaussian beam is given in Figure 6.23(a). As one may see, the fourth-order super-Gaussian increases the peak value of far-field irradiance by 1.6 times compared to the Gaussian TEM_{00} mode of the resonator. At the same time, however, the super-Gaussian causes side lobes in the far-field irradiance distribution. However, they are not very significant, so that the experimental M^2 factor for the fourth-order super-Gaussian mode is $M^2 = 1.36$. We would like to mention that for an "ideal" fourth-order super-Gaussian beam having the same near-field beam waist $\omega = 4.8$ mm, the M^2-factor is generally higher ($M^2 = 1.46$), as illustrated by curve 2 in Figure 6.11. In this case, it is seen

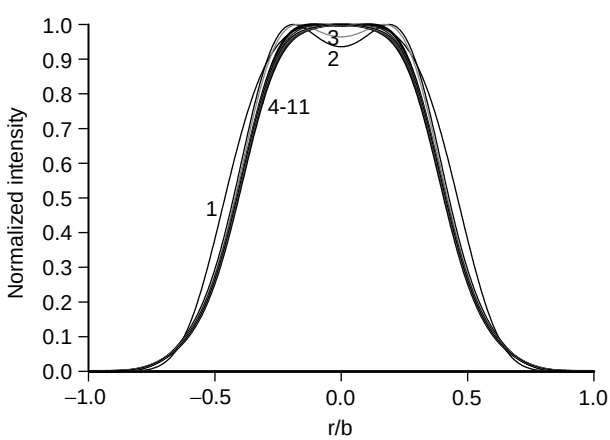

FIGURE 6.21 Evolution of the fourth-order super-Gaussian beam at the surface of the output mirror: 1 — initial beam, 2 — the beam after one round trip, 3 — after two round trips, 4 — after three round trips, etc., 11 — after ten round trips.

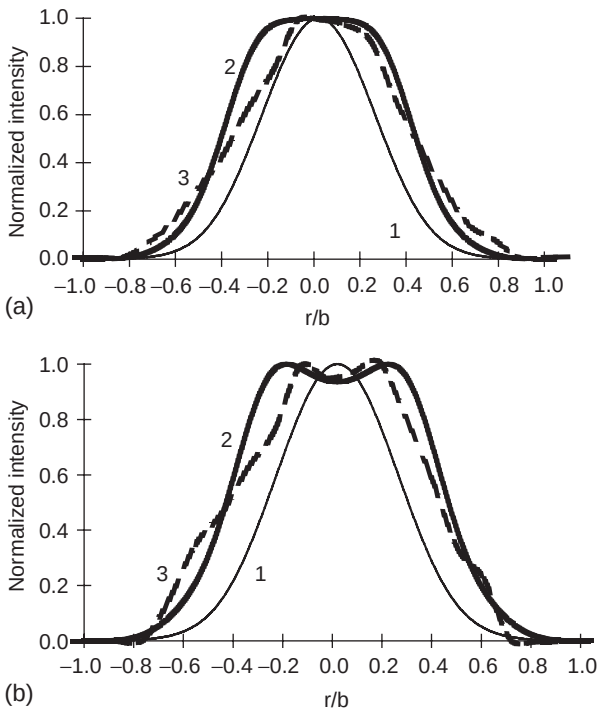

FIGURE 6.22 Formation of the super-Gaussian fundamental mode: (a) super-Gaussian fourth-order mode. 1 — Gaussian mode, 2 — theoretically obtained super-Gaussian fourth-order mode, 3 — experimentally obtained super-Gaussian fourth-order mode; (b) super-Gaussian sixth-order mode. 1 — Gaussian mode, 2 — theoretically obtained super-Gaussian sixth-order mode, 3 — experimentally obtained super-Gaussian sixth-order mode.

from Figure 6.11 that the width of the far-field beam increases because of the side lobes. For sixth-order super-Gaussian beams the difference is higher: the beam formed by the flexible mirror has $M^2 = 1.38$, while the ideal beam has $M^2 = 1.8$. So, the fact that the resonator with a corrector does not ideally reproduce the super-Gaussian function in the near-field (Figure 6.22) results in a positive effect in the far-field: the side lobes are reduced which improves the M^2-factor. We define the M^2-factor according to the international standard ISO 11146[25] as $M^2 = \pi d_0 \theta/(4\lambda)$; where λ is the wavelength, d_0 is the near-field waist diameter calculated as the second moment of the irradiance distribution at the waist location (in our case at the plane of the output resonator mirror)

$$d_0 = 2\sqrt{2}\frac{\int\int r^2 I(r,z) r\,\mathrm{d}r\,\mathrm{d}\varphi}{\int\int I(r,z) r\,\mathrm{d}r\,\mathrm{d}\varphi},$$

and θ is the divergence angle defined as $\theta = d_f/f$, where f is the focal length of lens and d_f is the beam width defined as the second moment of the focal plane irradiance distribution

$$I_f(r,z) : d_f = 2\sqrt{2}\frac{\int\int r^2 I_f(r,z) r\,\mathrm{d}r\,\mathrm{d}\varphi}{\int\int I_f(r,z) r\,\mathrm{d}r\,\mathrm{d}\varphi}.$$

Now we can come back to the experiment itself. To apply voltages to the electrodes of the flexible mirror we used a variable-voltage power supply (Figure 6.20; 1). The near-field irradiance distribution was observed with the help of a laser beam analyzer (LBA-2A; Figure 6.20; 8), and

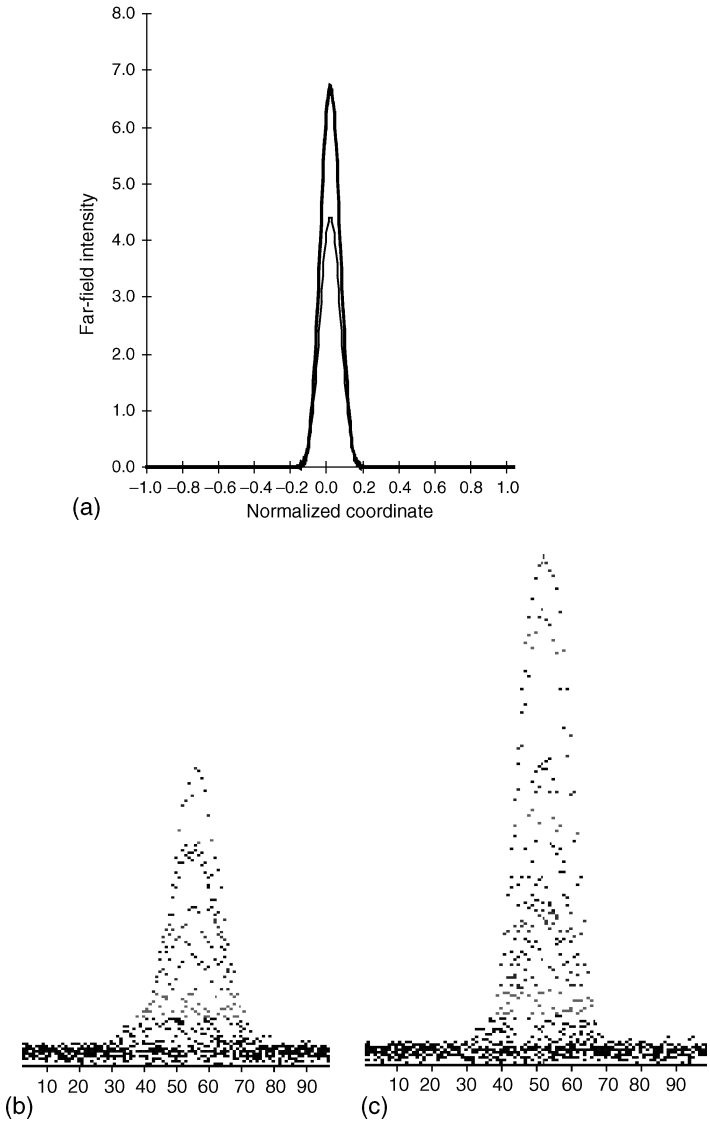

FIGURE 6.23 Far-field pattern of laser beam: (a) theoretically calculated Gaussian and fourth-order super-Gaussian modes; (b) experimentally obtained Gaussian TEM_{00} mode; (c) experimentally obtained super-Gaussian fourth-order TEM_{00} mode.

the far-field pattern (in the focal plane of lens; Figure 6.20; 11; $f = 275$ mm) was analyzed by a mode analyze computer (MAC-2; Figure 6.20; 12). The result of experimentally forming a fourth-order super-Gaussian beam is presented in Figure 6.22(a), curve 3. The total power of the formed super-Gaussian beam was about 10% higher than the power contained in the Gaussian beam, and the waist was widened by 1.26 ± 0.05 times (the calculations showed that it should have increased by 1.29 times). In the focal plane of lens (Figure 6.20; 11; far-field) the experimental irradiance profile for the Gaussian mode is given by Figure 6.23(b). The peak value of the far-field irradiance distribution for the fourth-order super-Gaussian beam (Figure 6.23(c)) is 1.6 times higher than that for the Gaussian beam. This fact is in good agreement with the theory as shown in Figure 6.23(a). The shape of the far-field pattern becomes narrower, but the side lobes that should

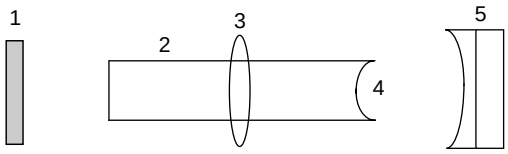

FIGURE 6.24 Schematic of a telescopic-type stable resonator for a YAG:Nd^{3+} laser with a wide-aperture mirror: 1 — output coupler, 2 — active medium, 3 — thermal lens, 4 — meniscus, 5 — bimorph flexible mirror.

exist are not distinguishable from the noise level. The near-field irradiance distribution for the experimentally formed sixth-order super-Gaussian beam is shown in Figure 6.22(b), curve 3. In this case we observed a 12% total power increase in comparison with the Gaussian fundamental mode. The observed far-field pattern for the formed sixth-order super-Gaussian mode is very similar to the one for the fourth order mode.

VII. YAG:Nd^{3+} LASER. FORMATION OF A SUPER-GAUSSIAN OUTPUT BEAM — NUMERICAL RESULTS

This section presents calculations aimed at investigating the formation of specified irradiance profiles for a YAG:Nd^{3+} laser. Active mirrors tend to have rather large-apertures — their diameter is 20 mm or larger. It is difficult to use such deformable mirrors in the cavities of industrial CW solid-state lasers because of the relatively small beam apertures in stable resonators. To solve this problem, we suggest expanding the beam inside the laser cavity up to the diameter of the adaptive mirror by using a meniscus on the one end of the gain element[26] (Figure 6.24). At the same time, the bimorph flexible mirror has a concave spherical profile. Such a laser resonator permits the use of wideaperture mirrors without any supplementary optical elements and therefore without undesirable loss. We considered the case of forming a super-Gaussian output with a resonator having the main parameters of Fresnel numbers $N_1 = b^2\backslash B\lambda = 0.3$ and $N_2 = a^2\backslash B\lambda = 12.3$, and geometric factor $G = 0.58$. Here, $2a = 20$ mm is the diameter of the bimorph deformable mirror, $2b = 6$ mm is the diameter of the plane output mirror, $\lambda = 1.06\ \mu$m is the wavelength, and $B = 6200$ mm is the effective length of the telescopic type of resonator (Figure 6.24). A, B, and D are the elements of the ray $ABCD$ matrix for the laser resonator.

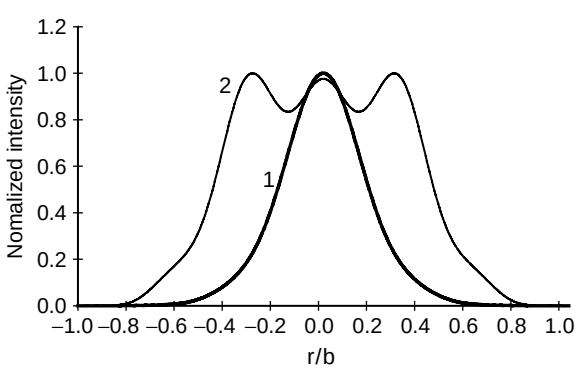

FIGURE 6.25 Formation of super-Gaussian fundamental modes at the output of a stable resonator in a YAG:Nd^{3+} laser: 1 — Gaussian mode, 2 — fourth-order super-Gaussian modes.

Figure 6.25 shows the results of the diffraction calculations. Curve 1 represents the Gaussian fundamental TEM_{00} mode at the resonator output while curve 2 shows the fourth-order super-Gaussian beam profile. Calculations show that the mode volume for the super-Gaussian beam increases by a factor of 2.1 to 2.2, diffraction losses decrease by 1.1 to 1.2 times, and the far-field peak irradiance increases by a factor of two in comparison with the Gaussian TEM_{00} mode. The mode volume was estimated as the average of transverse irradiance distributions calculated at five points inside the cavity and at the mirrors as well. Power losses δ were calculated as $\delta = |1 - \gamma_1 \gamma_2|$.

VIII. CONCLUSION

This chapter has shown the ability to form a specified irradiance output in both $YAG:Nd^{3+}$ and CO_2 laser resonators by means of an intracavity flexible mirror. The experiment with a CW CO_2 laser has shown that while remaining in the TEM_{00} regime, we were able to increase the total output power by 10 to 12% and to increase the peak value of far-field irradiance by 1.6 times in comparison with a Gaussian fundamental mode. This work opens the possibility of "intelligent" flexible lasers that generate irradiance distributions specified by the user.

ACKNOWLEDGEMENTS

The authors would like to thank personnel from the Group of Adaptive Optics for Industry and Medicine of the Institute of Laser and Information Technologies, Russian Academy of Sciences, for their help in fabricating and testing the mirrors and in carrying out experiments. Also, we are very grateful to Prof. L. N. Kaptsov and Prof. S. S. Chesnokov from Moscow State University for their helpful discussions. Finally, we wish to thank Scott C. Holswade for his assistance in editing the manuscript.

REFERENCES

1. Abil'sitov, G., ed., *Technological Lasers, Moscow*, 1991 (in Russian).
2. Koebner, H., ed., *Industrial Applications of Lasers*, Wiley-Interscience, New York, 1988.
3. Borghi, R., and Santarsiero, M., Modal structure analysis for a class of axially symmetric flat-topped laser beams, *IEEE J. Quantum Electron.*, 35, 745–750, 1999.
4. Santarsiero, M., and Borghi, R., Correspondence between super-Gaussian and flattened Gaussian beams, *J. Opt. Soc. Am A*, 16, 188–190, 1999.
5. Gory, F., Flattened Gaussian beams, *Opt. Comm.*, 107, 335–341, 1994.
6. Bollanti, S., Lazzaro, P. Di., Murra, D., and Torre, A., Analytical propagation of super-gaussian-like beams in the far-field, *Opt. Comm.*, 138, 35–39, 1997.
7. De Silvestri, S., Magni, V., Svelto, O., and Valentini, G., Lasers with super-Gaussian mirrors, *IEEE J. Quantum Electron.*, 26, 1500–1509, 1990.
8. Dainty, J. C., Koryabin, A. V., and Kudryashov, A. V., Low-order adaptive deformable mirror, *Appl. Opt*, 37(21), 4663–4668, 1998.
9. Anan'ev, Yu. A., In *Laser Resonators and the Beam Divergence Problem*, Higler, A., ed., 1992, Bristol.
10. McClure, E. R., Manufactures turn precision optics with diamond, *Laser Focus World*, 27, 95–105, 1991.
11. van Neste, R., Paré, C., Lachance, R. L., and Bélanger, P. A., Graded-phase mirror resonator with a super-Gaussian output in a CW-CO_2 laser, *IEEE J. Quantum Electron.*, 30, 2663–2669, 1994.
12. Kudryashov, A., and Shmalhausen, V., Semipassive bimorph flexible mirrors for atmospheric adaptive optics application, *Opt. Engng.*, 35, 3064–3073, 1996.
13. Kudryashov, A. V., and Samarkin, V. V., Control of high power CO_2 laser beam by adaptive optical elements, *Opt. Comm.*, 118, 317–322, 1995.
14. Baumhacker, H., Witte, K.-J., Stehbeck, H., Kudryashov, A., and Samarkin, V., In *Use of deformable mirrors in the 8-TW TiS-laser ATLAS*, Love, Gordon, ed., World Scientific, pp. 28–31, 2000.

15. Kudryashov, A. V., and Seliverstov, A. V., Adaptive stabilized interferometer with laser diode, *Opt. Comm.*, 120, 239–244, 1995.
16. Fox, A. G., and Li, T., Resonant modes in a maser interferometer, *The Bell Syst. Tech. J.*, 40, 453–488, 1961.
17. Li, T., Diffraction loss and selection of modes in maser resonators with circular mirrors, *The Bell Syst. Tech. J.*, May, 917–932, 1965.
18. Paré, C., and Bélanger, P. A., Custom laser resonators using graded-phase mirrors: circular geometry, *IEEE J. Quantum Electron.*, 30, 1141–1148, 1994.
19. van Neste, R., Paré, C., Lachance, R. L., and Bélanger, P. A., Graded-phase mirror resonator with a super-Gaussian output in a CW-CO_2 laser, *IEEE J. Quantum Electron.*, 30, 2663–2669, 1994.
20. Bélanger, P. A., Paré, C., Lachance, R. L., and van Neste, R., U.S. patent 5,255,283, 1993.
21. Bélanger, P. A., and Paré, C., Optical resonators using graded phase mirrors, *Opt. Lett.*, 16, 1057–1059, 1991.
22. Zakharova, G., Karamzin, Yu. N., and Trofimov, V. A., Some problems of optical radiation nonlinear distortions compensation. Blooming and random phase distortions of profiled beams, *Atmospheric Optics and Climate*, 8, 706–712, 1995.
23. Ahmanov, S. A., Vorontsov, M. A., Kandidov, V. P., Syhorykov, A. P., and Chesnokov, S. S., Thermal self-action of light beams and methods of its compensation, *Izv. Visshih Uchebnih Vavedenii*, XXIII, 1–37, 1980 (in Russian).
24. Q3 Galushkin, M. G., Golubev, V. S., Zavalov, Yu. N., Zavalova, V. Ye., and Panchenko, V. Ya., Enhancement of small-scale optical nonuniformities in active medium of high-power CW FAF CO_2 laser, In *Optical Resonators—Science and Engineering*, Kossowsky, R. et al., eds., Kluwer Academic Publishers, New York, pp. 289–300, 1998.
25. International Standard ISO 11146, Optics and optical instruments, Lasers and laser related equipment, Test methods for laser beam parameters: Beam widths, divergence angle and beam propagation factor. Document ISO/TC 172/SC 9/WC, 1995.
26. Cherezova, T. Yu., Kaptsov, L. N., and Kudryashov, A. V., CW industrial rod YAG:Nd3+ laser with an intracavity active bimorph mirror, *Appl. Opt.*, 35, 2554–2561, 1996.

Author Queries

JOB NUMBER: 9325

Title: Laser Beam Shaping by Means of Flexible Mirrors

Q1 Please check the definitions for the acronyms have been inserted correctly.

Q2 Please confirm 'Segnetomaterial' is correct.

Q3 Please provide complete list of author names for Ref. 24

Q4 Please check whether Figure 6.7 is ok.